Article ID: 1007－4627(2010)03－0229－23

New Insights into Frontier of Nuclear Structure of Neutron-rich Nuclei by Means of Prompt Fission γ Ray Measurements at Gammasphere (Ⅰ: Section 1 & Section 2)*

Y. X. Luo(罗亦孝)[1,2], J. H. Hamilton[1], J. O. Rasmussen[2], A. V. Ramayya[1], C. Goodin[1], A. V. Daniel[1,3,4], N. J. Stone[5,6], S. J. Zhu(朱胜江)[1,7], J. K. Hwang[1], S. H. Liu(刘少华)[1], C. J. Beyer[1], Ke Li(李 科)[1], H. L. Crowell[1], D. Almehed[8], S. Frauendorf[8,9], A. Covello[10], V. Dimitrov[11], Jing-ye Zhang(张敬业)[6], X. L. Che(车兴来)[7], Z. Jang(姜 卓)[7], D. Fong[1], A. Gelberg[12], I. Stefanescu[13], A. Gargano[10], E. F. Jones[1], P. M. Gore[1], I. Y. Lee[2], G. M. Ter-Akopian[3], Yu. Ts. Oganessian[3], M. A. Stoyer[14], R. Donangelo[15], W. C. Ma(马文超)[16], J. D. Cole[17], J. Kormicki[1], X. Q. Zhang(张学谦)[1], S. C. Wu[18], J. Gilat[2], T. N. Ginter[2,19], S. J. Asztalos[20]

(1 *Physics Department, Vanderbilt University, Nashville, TN* 37235, *USA*;
2 *Lawrence Berkeley National Laboratory, Berkeley, CA* 94720, *USA*;
3 *Flerov Laboratory for Nuclear Reactions, JINR, Dubna, Russia*;
4 *Joint Institute for Heavy Ion Research, Oak Ridge, TN* 37831, *USA*;
5 *Department of Physics, Oxford University, Oxford OX*1 3*PU, United Kingdom*;
6 *Department of Physics and Astronomy, University of Tennessee, Knoxville, Tennessee* 37996, *USA*;
7 *Physics Department, Tsinghua University, Beijing* 100084, *China*;
8 *Department of Physics, University of Notre Dame, Notre Dame, IN* 46556, *USA*;
9 *Institut für Strahlenphysik, FZD-Rossendorf, Postfach* 510119, *D*-01314 *Dresden, Germany*;
10 *Dipartimento di Scienze Fisiche, Universita di Napoli Federico II, and Istituto Nazionale di Fisica Nuclear, Complesso Universitario di Monte S. Angelo, Via Cintia*, 80126 *Napoli, Italy*;
11 *Idaho Accelerator Center, Idaho State University, Pocatello, ID*-83209-8263, *USA*;
12 *Institut für Kernphysik, Universität zu Köln*, 50937 *Köln, Germany*;
13 *Department of Chemistry and Biochemistry, University of Maryland, MD* 20742, *USA*;
14 *Lawrence Livermore National Laboratory, Livermore, CA* 94550, *USA*;
15 *Instituto de Física, Facultad de Ingeniería, C. C.* 30, 11300 *Montevideo, Uruguay*;
16 *Mississippi State University, Drawer* 5167, *Mississippi State, MS* 39762, *USA*;
17 *Idaho National Laboratory, Bldg. IRCPL, MS*2114, *Idaho Falls, ID* 83415, *USA*;
18 *Department of Physics, National Tsing Hua University, Hsinchu, Taiwan* 30013, *China*;
19 *National Superconducting Cyclotron Laboratory, Michigan State University*,

* **Received date**: 7 Apr. 2010; **Revised date**: 3 May 2010

* **Foundation item**: US Department of Energy Grants (DE-FG05-88ER40407, DE-FG02-96ER40983, DE-FG02-95ER40093) and Contract (W-7405-ENG48, DE-AC03-76SF00098, DE-AC07-76ID01570); The Work at Tsinghua University was supported by National Natural Science Foundation of China (10575057, 10775078); Major State Basic Research Development Program of China (2007CB815005)

Biography: Luo Yi-xiao(1944-), male(Han Nationality), Zigong, Sichuan, Researcher, working on nuclear structure; E-mail: yxluo@lbl.gov

East Lansing, *Michigan* 48824, *USA*;
20 *Massachusetts Institute of Technology*, *Cambridge*, *Massachusetts* 02139, *USA*)

Abstract (Section 1 and Section 2): New insights have been gained into the frontiers of nuclear structure of neutron-rich nuclei by means of γ-γ-γ and γ-γ(θ) coincidences of prompt γ rays emitted in the spontaneous fission of ^{252}Cf at Gammasphere. Over 5.7×10^{11} triple-and higher-fold coincidence events and the less-compressed cube data provide excellent conditions for searches and studies over a wide unknown range with more neutron excess. High-spin yrast and near yrast level schemes of neutron-rich nuclei in regions of physics interest have been identified for the first time, or extensively extended and expanded compared to previous preliminary measurements.

Chiral symmetry breaking was recently identified in even-even neutron-rich ^{110,112}Ru and ^{108}Mo isotopes. The former have the largest lowering of ground state energy when axial symmetry is broken, and near maximum triaxiality was deduced in the isotopes. By exhibiting all the fingerprints for chiral doubling, especially the best energy degeneracy, the doublet bands observed in these Ru and Mo isotopes are the best examples of chiral properties reported in this region. The evolution of chirality from γ-soft ^{108}Ru to triaxial ^{110,112}Ru is proposed. Tilted axis cranking (TAC) calculations extended by random phase approximation (RPA) calculations can explain the features of the doublet bands in terms of a soft chiral vibration for these even-even nuclei. The chirality in these even-even nuclei cannot be reduced to the simple geometrical picture as in odd-odd nuclei. Instead, in these even-even nuclei the tendency to chirality comes about from the interplay of all the neutrons in the open shell.

Systematic studies of the $N=83$ isotonic chain in the vicinity of the doubly-magic ^{132}Sn have yielded a wealth of spectroscopic information in this attractive region. The new data of $N=83$ isotones ^{135}Te ($Z=52$), ^{136}I ($Z=53$), ^{137}Xe ($Z=54$), ^{138}Cs ($Z=55$) and ^{139}Ba ($Z=56$), especially the observation of the long-sought level scheme of ^{138}Cs, and shell model calculations, indicate the key role played by the coupling of the excitations of the few $g_{7/2}$ valence protons outside the $Z=50$ major shell closure and the $f_{7/2}$ valence neutrons outside the $N=82$ major shell closure. Resemblance of spectroscopy and counterparts were observed between the ^{132}Sn region and ^{208}Pb region. Tilted rotation(magnetic rotation) was observed in ^{135}Te, which is the first observation of magnetic rotation in the vicinity of ^{132}Sn.

Key words (Section 1 and Section 2): neutron-rich nuclei; high spin; yrast; fission; ^{252}Cf; γ-γ-γ and γ-γ(θ) coincidences; Gammasphere; chiral symmetry breaking; triaxiality; tilted axis cranking (TAC) calculations; soft chiral vibration; $N=83$ isotonic chain; doubly-magic ^{132}Sn; shell model calculation; magnetic rotation; similarities of spectroscopy

CLC number: O572.33 **Document code**: A

Searches and studies of neutron-rich nuclei have opened a new era of nuclear spectroscopy. The β^- decay of fission products, thermal neutron capture, (d, p), (t, p), (α, xn) and heavy ion induced fission, incomplete fusion, and deep inelastic reaction have been used to populate low (in some cases to medium) spins in neutron-rich nuclei. However, the broad and detailed exploration of the high spin yrast and near-yrast spectroscopy of the neutron-rich nuclei had not been realized until the advent of large γ-detector arrays in combination with fission source[1, 2]. Measure-

ments of prompt γ rays from fission by the multi-detector arrays, such as Gammasphere and EUROGAM, have covered a vast range of previously unknown neutron-rich nuclei.

The most recent progress in the spectroscopy of neutron-rich nuclei made by our collaboration are based on the two experimental runs each taking two weeks in 2000, in which a ^{252}Cf source of 62 μCi, sandwiched between two 10 mg/cm^2 Fe foils, was placed in an 8-cm-polyethylene ball centered in the Gammasphere[3] which had 101 Compton-suppressed Ge detectors active. Over 5.7×10^{11} triple and higher-fold events were accumulated. The Radware cube three-dimensional histogram and less-compressed cube with one-third less compression[4] created based on these high statistics and high quality triple coincidence data provided the key conditions to explore the unknown neutron-rich regions.

The identification of a new transition in a nucleus was based on cross-checking the coincident relationships with its low-lying known transitions (if any) and with those of its complementary fission partners. Additional evidence for assignment of a transition to a nucleus can be obtained by measuring the fission yield ratios of the transition in the nucleus to another transition in its neighboring known isotope in gated spectra with gates set on its fission partner isotopic chain, 3n, 4n and 5n fission partners, respectively. The variations of the fission yield ratios with gates set on the 3n, 4n and 5n fission partners, respectively, were compared to those known ratios of ^{144}Ba and ^{143}Ba in ^{103,104,105}Mo gates(3n, 4n and 5n fission partners of ^{144}Ba)[5,6]. The consistent variations of the fission yield ratios provided additional evidence for the assignment of the transition to the nucleus.

Transition energies, relative intensities of γ transitions and branching ratios of levels were determined by peak-fittings[4] with proper background subtractions, which is crucial for fission γ data analysis.

The assignments of spin/parity to levels identified in a nucleus were based on angular correlation measurements[7], internal conversion coefficients (ICC) measurements, level systematics in neighboring isotopic and isotonic chains, decay patterns, and, where available, on theoretical model calculations.

This paper reviews the progresses in four hot topics at the frontier of nuclear spectroscopy of neutron-rich nuclei. Each section will first outline the major achievements and current interest in the research field, and then introduce the most recent progress made by our collaboration. The studies of chiral symmetry breaking in neutron-rich Ru, Mo isotopes, new spectroscopy of the $N=83$ isotonic chain in the vicinity of ^{132}Sn, new insight into the shape transitions and onset of deformation in $A\sim100$ region, and the recent detailed investigation of octupole excitations around $Z=56$, $N=88$ island and the observation of sharp drops in electric dipole moments in ^{141,143,144}Cs, and likely also in the La isotopic chain, are reviewed in Sections 1, 2, 3 and 4, respectively. Figures, tables and references are independently numbered in each of the four sections; and concluding remarks are given at the end of each section.

1 Chiral Symmetry Breaking in Neutron-rich ^{110,112}Ru and ^{108}Mo: the Best Examples of Chiral Doubling so far Reported in Nuclei, and the Evolution of Chirality from γ-soft ^{108}Ru to Triaxial ^{110,112}Ru

1.1 Introduction

The word "chiral" is a word of Greek origin, "chaire", which means "hand". Chirality is the study of handedness, right-handed and left-handed symmetry. Systems that can form right- and left-handed systems on reflection are chiral. For a long time, chiral structures have been of interest in complex molecules and elementary particles. The

right- and left-handed molecules have slightly different energies to give rise to energy doublets. They are related to each other by mirror reflections (see Fig. 1). The DNA double-helix and other complex bio-molecules are chiral. Although two enantiomers with the same binding energy exist for DNA, only one is synthesized.

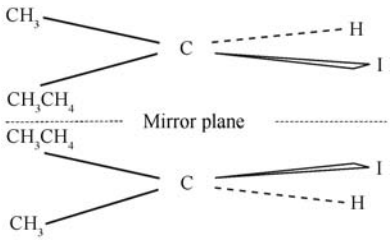

Fig. 1 Two chiral molecular states of the two enantiomers of 2-iodobutene. The broken line indicates the mirror plane.

However, the nucleus had long been thought to be achiral until Frauendorf and collaborators predicted the chiral symmetry breaking in rotating atomic nuclei with well-deformed triaxial shapes[8, 9]. The simplest case for chirality is an odd-odd triaxial nucleus where the total angular momentum vector is out of the three principal planes spanned by the three axes, and consequently there are significant components of angular momentum along each of the three axes. In such an odd-odd triaxial nucleus, when a high j particle aligns along the short axis (with Fermi level lying in the lower part of a valence particle high-j subshell), a high j hole along the long axis (with Fermi level lying in the upper part of a valence particle high-j subshell), and the rotational angular momentum along the intermediate axis, the three angular momentum vectors may couple to each other in a right- or left-handed way generating a chiral, right- or left-handed, system in the intrinsic frame (see Fig. 2).

Well-deformed triaxial deformations and configuration criteria are thus the characteristic conditions for generating chiral symmetry breaking in rotating nuclei.

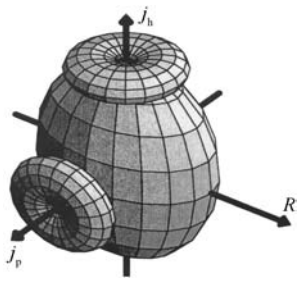

Fig. 2 A traxial odd-odd nucleus with a proton orbital and a neutron-hole orbital aligned, respectively, along the short and long principal axes, and the rotational angular momentum along the intermediate axis.

The spontaneous formation of the right- and left- handed system in a nucleus would give rise to nearly degenerate $\Delta I=1$ doublet bands in the laboratory frame. These chiral doublet bands exhibit a series of fingerprints[10, 11]: (A) Near energy degeneracy observed for partner levels, levels of the same spin/parity; (B) Similar structure, consequently similar electromagnetic properties such as $B(E2)/B(M1)$ ratios for partner levels; (C) Constant with spin and equal values of the energy staggering parameter $S(I)=[E(I)-E(I-1)]/2I$ for the two doublet bands, being due to the reduction of Coriolis interaction in the chiral doubling. In contrast to the ideal case generating chiral rotation, the still noticeable energy differences between the partner levels of the chiral doublet bands point to a dynamical character of chirality.

The theoretical predictions for chiral symmetry breaking in nuclei were followed by intensive experimental searches for chiral doublets in nuclei with triaxial deformations and fulfilling configuration criterion. Chiral doublets were first reported in ^{134}Pr[12, 13], and then in this $A\sim 130$ region in ^{136}Pm, ^{138}Eu[14], ^{130,132}La, ^{132}Pr[15, 16], ^{135,136}Nd[17, 18] and ^{124,126,128,130,132,134}Cs[19, 20], and in $A\sim 105$ region in ^{103,104,105,106}Rh[11, 21—23] and ^{100}Tc[24]. It was suggested[11] that the best observed chiral properties at that time were in ^{104}Rh. ^{106}Mo was reported by Zhu et al. of our collaboration to be the first even-even nucleus to have chiral symmetry breaking[25], in which chiral vibration

was proposed. Recently, the effect of γ-softness on the stability of chiral doubling was discussed for ^{106}Ag[26]. Based on B(E2) arguments possible misinterpretation of doublets as chiral was reported for ^{134}Pr[27]. However, lifetimes and electromagnetic transition probabilities of the two bands in ^{134}Pr were measured and investigated in the two-qp triaxial rotor and Interacting Boson Fermion Fermion (IBFF) models. The doublet bands in the nucleus were attributed to weak chirality dominated by shape fluctuations[28]. Recently the doublet bands in ^{135}Nd were associated with a transition from a vibrational to a static chiral region[29].

In contrast to the case of odd-odd nuclei, the investigations of the chiral doublet structure for odd-A ^{135}Nd[19, 20] and ^{105}Rh[21] revealed that the chiral symmetry breaking in odd-A nuclei are related to the two high-j particles aligned with the short axis of the triaxial nucleus. For even-even nuclei, the observation of chiral doublet bands seems to further exemplify the general geometric character of chiral symmetry breaking[9], because the non-planar geometry of rotation cannot be directly related to the alignment of high-j particles and holes with different principal axes[25] (also see the discussions below).

Motivated by the characteristic conditions for generating chirality, intensive search and studies of chiral symmetry breaking were performed in $^{108, 110, 112}$Ru and ^{108}Mo by our collaboration, and the best example of chiral properties of chiral doublet bands so far reported have been identified in $^{110, 112}$Ru[30, 31], ^{108}Mo, and in the previously reported ^{106}Mo[25]. Evolution of chirality from γ soft ^{108}Ru to triaxial $^{110, 112}$Ru is proposed[30].

1.2 The intensive searches for chiral symmetry breaking in neutron-rich $^{108, 110, 112}$Ru[30, 31] and ^{108}Mo

1.2.1 The characteristic conditions for generating chiral symmetry breaking in neutron-rich Ru, Mo isotopes

In an earlier work[32], theoretical calculations of Hartree-Fock energy surfaces for low-lying states in Ru isotopes suggested that the minimum nuclear shape starts near prolate spheroidal but migrates toward triaxial as one goes from mass 108 to 110 and 112 in Ru. In our systematic studies of the high-spin level structure of odd-Z isotopes $^{99, 101}$Y ($Z=39$), $^{101, 103, 105}$Nb ($Z=41$), $^{105-111}$Tc ($Z=43$), and $^{111, 113}$Rh ($Z=45$) (Refs. [33—36], also see the following Section 3) we found a smooth evolution in the triaxial parameter γ from $\gamma=0$ (axial symmetry) in $^{99, 101}$Y to $\gamma=-28°$ (near maximum triaxiality) in $^{111, 113}$Rh. From their global calculations of axial symmetry breaking in nuclear ground states, Möller et al.[37] have found three energy minima of the ground level energies centered around ^{149}Gd, ^{198}Pt and ^{108}Ru, with the region centered around ^{108}Ru, $Z=44$, $N=64$, as having the largest lowering of the nuclear ground-state energy when axial symmetry is broken. The appearance of a triaxial shape was also independently suggested by Stefanescu et al. of our collaboration[31]. In the calculations the ground-state band and one-phonon γ band energies and B(E2)'s in $^{108, 110, 112}$Ru were reproduced by the interacting boson model version IBM1-V3 which includes higher order terms to account for triaxiality[38]. A rigid triaxial rotor is suggested for $^{110, 112}$Ru. In addition, total Routhian surface (TRS) calculations of our collaboration suggest γ values of $-22°$, $-25°$ and $-59°$ at $\hbar\omega=0.0$ MeV, and $-27°$, $-32°$, $-39°$ at $\hbar\omega=0.4$ MeV in ^{108}Ru, ^{110}Ru and ^{112}Ru, respectively[39].

The experimental and theoretical studies have thus shown convincing evidence for the well-deformed triaxial shapes in these Ru/Mo isotopes. Neutron-rich Ru, Mo ($Z=44$, 42) isotopes are therefore good candidates of chiral symmetry breaking. The tilted axis cranking (TAC) calculations predicted that the chiral doublet bands in the isotopes can be built on the $\nu h_{11/2}\otimes(d_{5/2}g_{7/2})^{-1}$ configuration, which will have odd-parity.

1.2.2 Observations of the $\Delta I=1$ odd-parity dou-

blet bands in ^{108,110,112}Ru and ^{108}Mo

The high statistics triple-coincidence data at Gammasphere and the less-compressed cube are the key conditions to identify the very weakly populated odd-parity doublet bands with rich depopulation paths in ^{108,110,112}Ru and ^{108}Mo.

The identifications of the doublet bands of ^{108,110,112}Ru (and ^{108}Mo) were achieved by cross-checking the coincident relationships of the band transitions with those of the fission partners Xe (Ba for ^{108}Mo) isotopes and with their own related lower-lying transitions.

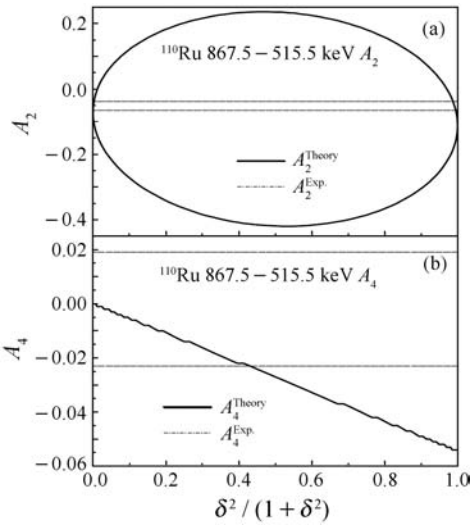

Fig. 3 An example of the γ-$\gamma(\theta)$ angular correlation data analyses. Experimental t-standard deviation limits on A_2 and A_4 coefficients are compared with the theoretical values to assign probable multipolarity of the depopulating 867.5 keV transition of the 2242.9 keV level of ^{110}Ru. See text.

Angular correlation measurements[7] were made at Gammasphere to assign multipolarities of the depopulating transitions and spins of the bandheads. The depopulating transitions of the bandheads of all the doublet bands were found to be pure dipole, and the spins of the bandheads were thus assigned. Fig. 3 shows an example of the γ-$\gamma(\theta)$ data analyses. For the 867.5−515.5 keV depopulating cascade of the 2242.9 keV level of ^{110}Ru, the 6-5-3 cascade (867.5−515.5 keV) with the 5 and 3 being known, has $A_2 = -0.052(14)$, $A_4 = 0.002(21)$, and theoretical $A_2 = -0.071$, $A_4 = 0$ for pure dipole for a $6^- - 5^-$ transition and $A_2 = -0.007$, $A_4 = -0.023$ for pure quadrupole. Spin 6 was thus assigned to the 2242.9 keV level, and pure dipole to the 867.5 keV transtion. Odd-parity was assigned to the level and supported by the unique decay paths. All of the band heads are measured to have lifetimes less than 1 ns so these can not be high K rotational bands.

Based on the coincidence relationship, balance of relative intensities, and angular correlation measurements, $\Delta I = 1$ doublet bands assigned odd-parity were identified in ^{108,110,112}Ru and ^{108}Mo. They are very weakly populated and show similar level patterns and decay patterns.

The level schemes showing the $\Delta I = 1$ odd-parity doublet bands, band 4, 5, 6, and 7, are reported for ^{108,110,112}Ru (Figs. 4, 5 and 6, respectively). The level scheme of ^{108}Mo is shown in Fig. 7, in which the doublet bands are not extended as high as in ^{108,110,112}Ru. The assignments of odd-parity to the doublet bands are in agreement with the predictions for chiral doubling in the Ru isotopes by TAC calculations. All the even-parity bands in ^{108,110,112}Ru not discussed in this review are reported in Ref. [39], where the ground-state bands (band 1 in the figures), γ-vibrational bands (band 2) and two-phonon γ-vibrational bands(band 3) are identified in ^{108,110,112}Ru (for ^{108}Ru, only the bandhead of the two-phonon γ-vibrational band is identified).

It can be seen from the level schemes that in the $\Delta I = 1$ odd-parity doublet bands, each spin/parity combination occurs twice, forming doublets. The lower levels of the doublet bands decay out via rich depopulation paths, feeding the ground band (band 1), one phonon γ band (band 2) and two phonon γ band (band 3). The highly branching of the decay out paths were challenging for the identifications of the weakly populated doublet bands, but, however, the decay patterns uniquely support the spin/parity assignments.

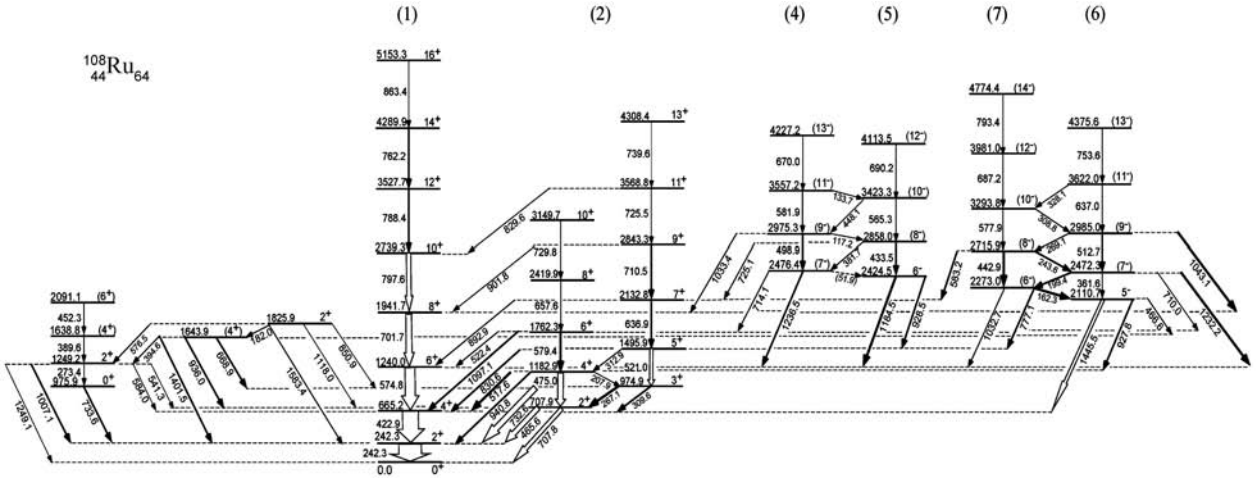

Fig. 4　Level scheme of ^{108}Ru with the $\Delta I=1$ odd-parity doublet bands (band 4, 5, 6, 7) identified[30, 31].

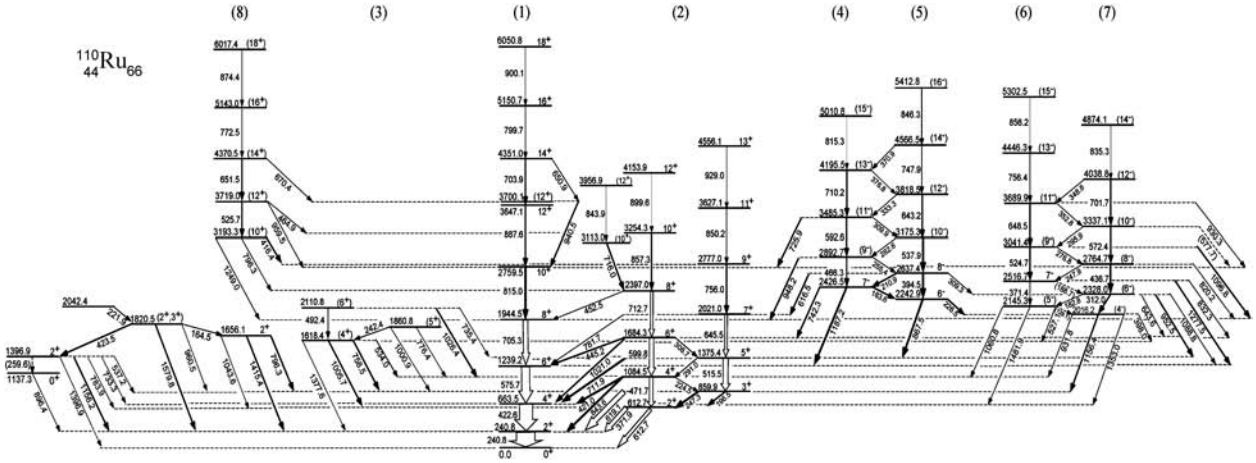

Fig. 5　Level scheme of ^{110}Ru with the $\Delta I=1$ odd-parity doublet bands (band 4, 5, 6, 7) identified[30, 31].

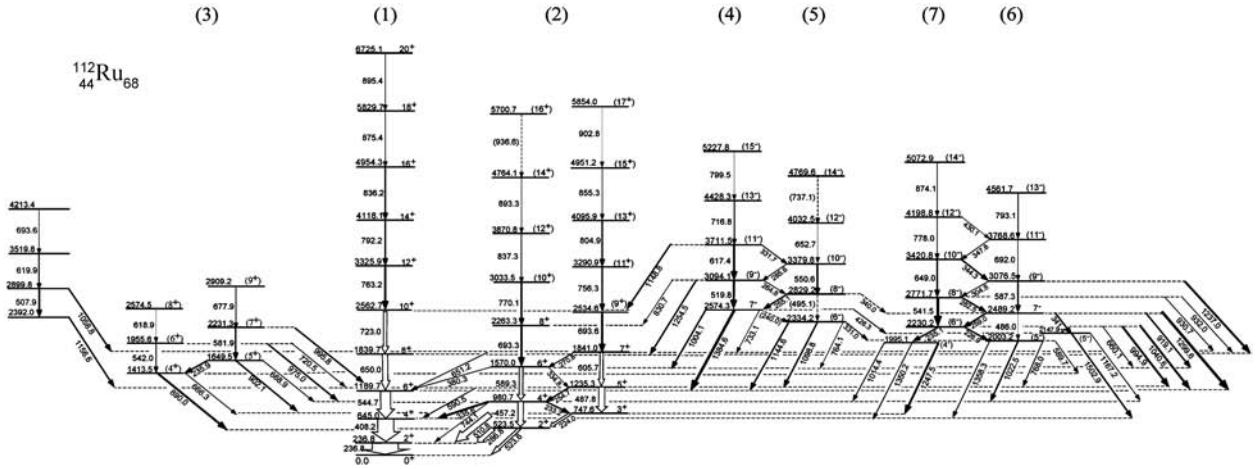

Fig. 6　Level scheme of ^{112}Ru with the $\Delta I=1$ odd-parity doublet bands (band 4, 5, 6, 7) identified[30, 31].

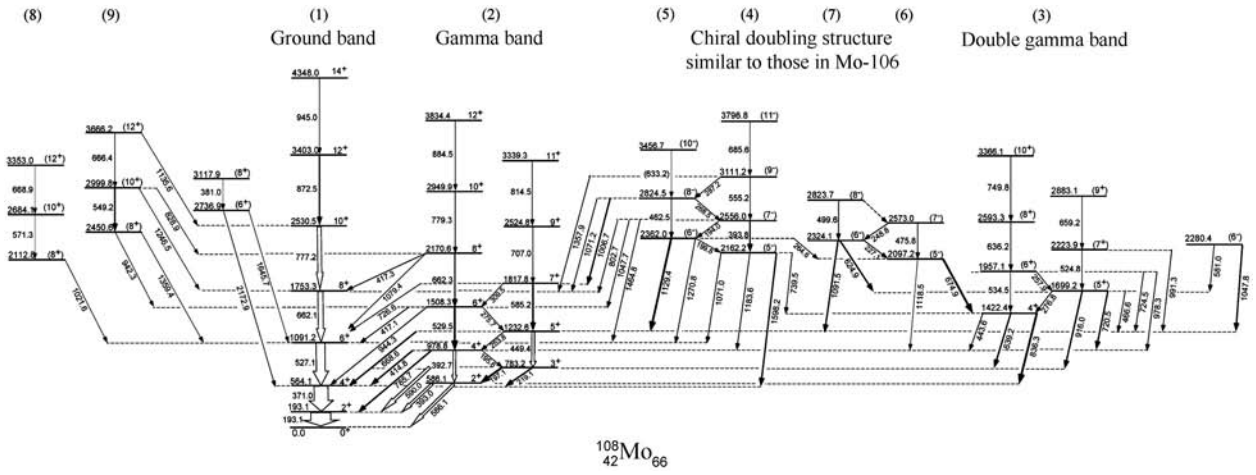

Fig. 7 Level scheme of ^{108}Mo with the $\Delta I=1$ odd-parity doublet bands (band 4, 5, 6, 7) identified.

1.2.3 Discussions of evidence for chiral symmetry breaking in ^{110,112}Ru and ^{108}Mo, and the evolution of chirality from γ soft ^{108}Ru to triaxial ^{110,112}Ru

As mentioned in the 1.2.1 subsection, the characteristic conditions for generating chiral symmetry breaking in nuclei, especially the well-deformed triaxial shapes, are surely fulfilled in Ru/Mo isotopes. In the following, the tests for fingerprints of the chiral symmetry breaking have shown that the $\Delta I=1$ odd-parity doublet bands observed in ^{110,112}Ru and ^{108}Mo are indeed chiral doublet bands, and they are the best examples of chiral nuclei reported so far.

A. Level excitations ~ spin plots

Level excitations of the doublet bands are plotted against spin in Fig. 8. One can see a pronounced smoothness and similar trend for the partner bands in ^{110,112}Ru, as expected for chiral doubling. This smoothness of the excitations can also be seen in the doublet bands in ^{108}Mo (not shown in the figure). However, one sees a crossing between band 4 & 5 and band 6 & 7 in ^{112}Ru, which may not strictly fit the ideal case of chiral doubling. The crossing in ^{112}Ru was interpreted as chiral instability in the nucleus (see the following 1.2.4 Subsection of theoretical calculations). However, the crossover may also be accounted for by a two-shape phenomenon: The TRS calculations of energy contours in the β-γ shape plane (by Zhu et al. of our collaboration[39]) show that the energy minimum for ^{112}Ru is an oblate spheroid at zero cranking and goes over to a triaxial minimum at higher cranking. A similar crossing was observed in ^{106}Ag[24], and one sees that ^{104}Rh also nearly crosses over at the upper end of the known bands[11]. According to Joshi et al.[26], this crossover occurs because triaxial and axial prolate shapes are very close in energy for ^{106}Ag, and possibly also for ^{104}Rh.

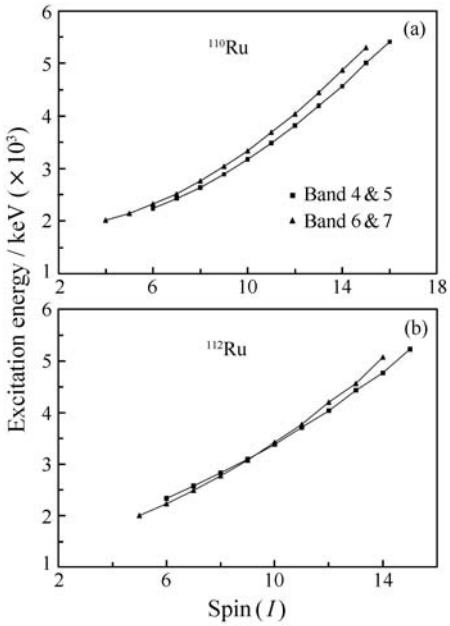

Fig. 8 Excitations ~ spins plot for the levels of the $\Delta I=1$ odd-parity doublet bands in ^{110,112}Ru.

In contrast to the smoothness seen in thd odd-parity bands of ^{110,112}Ru, the odd-parity bands of a large staggering of level excitations was observed in ^{108}Ru, which is not shown in Fig. 8, but can be

seen in Fig. 8(c) of Ref. [31]. This staggering is in fact more clearly seen in signature splitting and will be discussed in the following.

B. The energy staggering parameter $S(I)$ and the likely evolution of chirality from γ soft ^{108}Ru to triaxial ^{110,112}Ru

The energy staggering parameters $S(I)=[E(I)-E(I-1)]/2I$ for doublet bands in ^{110,112}Ru are shown in Fig. 9. It can be seen in the figure that the energy staggering parameters $S(I)$ are equal and constant with spin for the doublet bands, as expected for chiral symmetry breaking. In fact the energy staggering parameters $S(I)$ are small and smooth in ^{110,112}Ru, and comparable to those of ^{106}Rh, the latter being suggested more recently[22,26] to be the best example of a chiral nucleus.

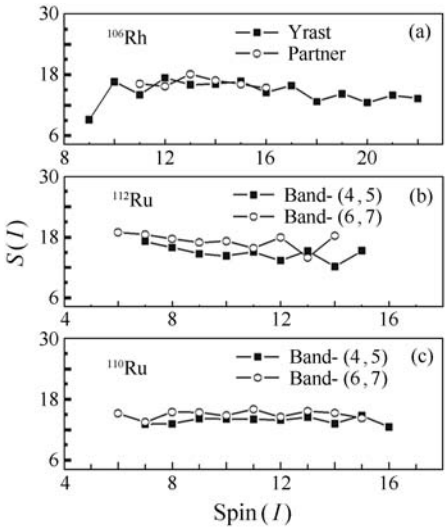

Fig. 9 Energy staggering parameter $S(I)$ for doublet transitions in ^{110,112}Ru and ^{106}Rh. The doublet bands observed in ^{106}Rh were suggested[22,26] to be the best example of chiral bands.

However, in contrast to ^{110,112}Ru and ^{106,108}Mo the non-yrast bands 4, 5 in ^{108}Ru develop a strong even-odd spin level-energy staggering (signature splitting) (see Fig. 10) whereas bands 6, 7 represent a good $\Delta I=1$ sequence without much staggering. This interesting difference between ^{108}Ru and ^{110,112}Ru was investigated by calculations and fittings to the level excitations, $B(E2)$'s and signature splittings of the ground-state band and one-phonon γ band using the standard IBM1 model and the version IBM1-V3 which includes higher order terms to account for triaxiality[38]. The fits suggest that ^{108}Ru is a γ soft $SU(6)$ nucleus well reproduced by the standard IBM1 model, and ^{110,112}Ru are more like rigid triaxial rotors well fitted by version IBM1-V3. These results are based on the observations that the odd-even spin staggering in the one phonon γ band in ^{108}Ru is exactly opposite to those in ^{110,112}Ru (see Fig. 11). Best fitting were obtained by the rigid triaxial rotor model IBM1+V3[38] in both ^{110,112}Ru, and the data of ^{110,112}Ru can not be reproduced by the standard IBM1, which implies that ^{110,112}Ru are most likely rigid triaxial rotors.

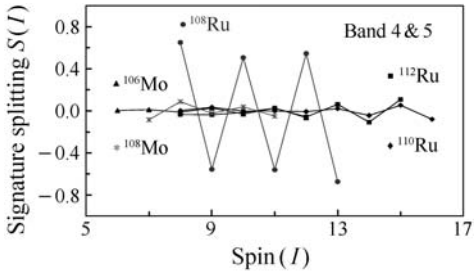

Fig. 10 Signature splitting of the bands 4 & 5 in ^{108,110,112}Ru. Those of ^{106,108}Mo, are also shown. While small and nearly constant signature splittings are seen in ^{110,112}Ru and ^{106,108}Mo, as expected for chiral symmetry breaking, a dramatic staggering is seen in ^{108}Ru. See text.

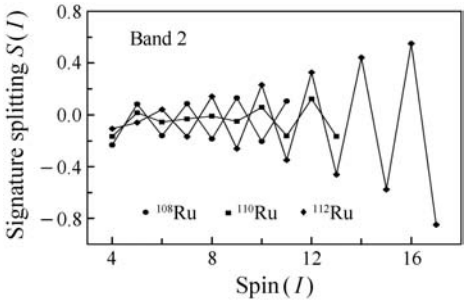

Fig. 11 Experimental signature splittings of the one phonon γ band (band 2) in ^{108,110,112}Ru[39]. The staggering in ^{108}Ru is exactly opposite to those in ^{110,112}Ru, interpreted as γ softness in ^{108}Ru. See text.

More likely the strong even-odd spin level-energy staggering observed in band 4 and 5 in ^{108}Ru is a consequence of the γ softness disturbing the chiral doublets. It is worth noting that a similar difference of odd-even spin staggering between the yrast and non-yrast doublet bands was found in γ soft ^{106}Ag[26], and attributed to different values of γ and shapes. It is therefore very interesting to have likely observed an evolution of chirality from γ soft ^{108}Ru to triaxial ^{110,112}Ru!

C. Electromagnetic properties, $B(E2)/B(M1)$ ratios of the doublet bands observed in ^{110,112}Ru

Table 1 compares the $B(E2)/B(M1)$ ratios of the $\Delta I=2$(E2) to $\Delta I=1$(M1+(E2)) strengths for the doublet bands in ^{110,112}Ru and ^{134}Pr. Since the doublet bands in ^{108}Mo are not extended high enough its ratios are not available. The $\Delta I=1$ transitions are assumed to be M1. In ^{110,112}Ru the $B(E2)/B(M1)$ ratios for each partner level are in reasonable agreement, which indicates that the doublet bands in ^{110,112}Ru have very similar structures as required for chiral doublets. For comparison, the ratios for ^{134}Pr differ by 2.5 to 7.6 for the two bands (cf. Table 1). Substantial differences between the in-band $B(E2)$ values of the two chiral partners in ^{134}Pr were observed and considered as evidence for a possible misinterpretation of nearly degenerate pairs of bands as chiral partners[27].

Table 1 $B(E2)/B(M1)$($e^2b^2/\mu_N{}^2$) ratios in doublet bands 4—5 and 6—7 in ^{110,112}Ru and bands 1—2 in ^{134}Pr

^{110}Ru			^{112}Ru		^{134}Pr		
Spin(I)	4—5	6—7	4—5	6—7	Spin(I)	1	2
13	>1.3				18	0.48	
12	3.1	1.6	>1.1	1.4	17	0.55	0.08
11	2.4	4.4	2.9	1.5	16	0.80	0.14
10	3.5	2.1	2.6	2.5	15	0.48	0.19
9	2.5	4.2	5.1	3.4	14	0.38	0.05
8	2.6	3.3		2.0	13	0.25	

The microscopic TAC calculations described in the following section give very different (factor of 10) $B(E2)/B(M1)$ ratios for different configurations. Thus these similar $B(E2)/B(M1)$ values rule out the possibility that these new doublets originate from two accidentally degenerate configurations from the coupling of say an $h_{11/2}$ neutron to two different neutron bands in ^{109,111}Ru.

D. Energy degeneracy in the $\Delta I=1$ odd-parity doublet bands in ^{110,112}Ru and ^{108}Mo——the most nearly degenerate doublet bands observed so far

Energy degeneracies of the $\Delta I=1$ odd-parity doublet bands observed in ^{110,112}Ru and ^{108}Mo are shown in Fig. 12. In the figure the energy differences between the partner levels for ^{110,112}Ru, ^{106,108}Mo and ^{104,105,106}Rh are plotted against spins for comparison. Note that the energy differences in ^{110,112}Ru and ^{106,108}Mo are considerably smaller than those of ^{104,106}Rh, the latter being suggested to be the best examples of chiral doublets[11,26]. The tests for energy degeneracy in ^{110,112}Ru and ^{106,108}Mo indicate that the doublet bands observed in these Ru/Mo isotopes are best examples of chiral properties reported so far.

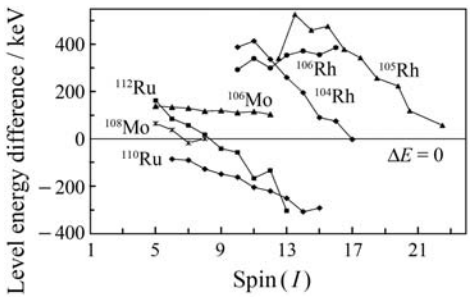

Fig. 12 Energy difference of the partner levels of the doublet bands in ^{110,112}Ru, ^{106,108}Mo and ^{104,105,106}Rh. Considerably smaller energy differences are seen in ^{110,112}Ru and ^{106,108}Mo in comparison with those in ^{104,106}Rh, the latter being reported before to be the best example of chiral properties.

The still noticeable energy splitting in ^{110,112}Ru points to a dynamical character of chirality, being intermediate between a slow vibrational excursion into left-and right-handed regions and a tunneling motion between the two regions.

1.2.4 The Tilted Axis Cranking (TAC) and Random Phase Approximation (RPA) calculations

Tilted axis cranking (TAC) and random phase approximation (RPA) calculations were performed for different two-quasi neutron configurations in ^{110}Ru and ^{112}Ru. The results are quite similar for both nuclei. The combination of the TAC method with RPA is described in detail in Ref. [40], where it is applied to odd-odd nuclei. The method has been used successfully to describe the chiral vibration in ^{135}Nd[29]. A self-consistent TAC Hamiltonian in a harmonic oscillator basis with the *QQ*-force in three major harmonic oscillator *N*-shells ($N_{\rm low}=3$ and $N_{\rm up}=5$) was used.

$$H'=h_0+\sum_{m=-2}^{2}\frac{\kappa_0}{2}\sum_{N=4}^{5}\bar{Q}_m^{(N)}\bar{Q}_m^{(N)}(-)^{m+1}-\Delta(P^++P)-\boldsymbol{\omega}\cdot\boldsymbol{J}\ , \qquad (1)$$

where h_0 is the spherical Woods-Saxon energy[41]. The

$$\bar{Q}_m^{(N)}=\left(\frac{N_{\rm low}-B}{N-B}\right)\left(\frac{2A_{\rm n(p)}}{A}\right)^{1/3}Q_m^{(N)} \qquad (2)$$

are the dimensionless quadrupole operators for each *N*-shell multiplied by a *N* and isospin dependent quenching factor[40, 41], and $A_{\rm n(p)}$ are the neutron and proton numbers, i. e. $A=A_{\rm n}+A_{\rm p}$. We use the values of κ_0 (0.0605 [MeV]) and B (-0.5) that give a good agreement with data on the ground-state band and the energy of the γ vibration.

Since the two-quasi proton states lie at higher energy than the two-quasi neutron states in this region, our new negative parity bands are interpreted as two-quasi neutron excitations. The lowest configuration is obtained by exciting a neutron from the highest $h_{11/2}$ level to the low-lying mixed $d_{5/2}$—$g_{7/2}$ levels. The microscopic TAC calculations give a total routhian (energy in the rotating frame), which depends only very weakly on the orientation of the rotational axis with respect to the triaxial shape. This softness cannot be reduced to the simple picture discussed for odd-odd nuclei, where instability toward a non-planar orientation of the rotational axis is the consequence of combining a high-*j* particle and a high-*j* hole with collective rotation. The tendency to chirality comes about from the interplay of all the neutrons in the open shell, and we could not find a simple partition.

The soft energy surface obtained from the mean field calculations implies a low-lying collective mode in the orientation degree of freedom, i. e. a soft chiral vibration. Thus, we interpret the bands 6, 7 as the zero-phonon state, which is given by the TAC solution, and bands 4, 5 as the one-phonon state, which is given by the RPA solution. The results of the TAC and RPA calculations are plotted in Fig. 13 together with the experimental data.

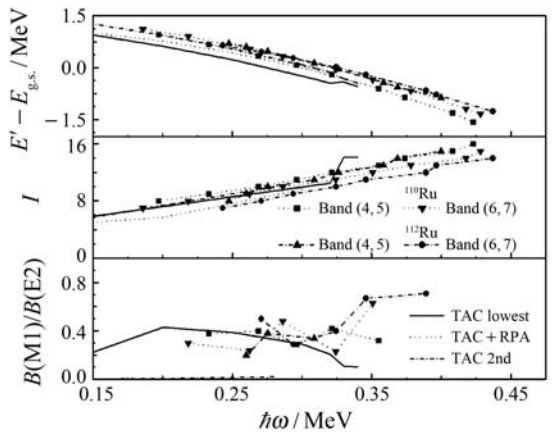

Fig. 13 Energy in the rotating frame (upper panel), angular momentum (middle panel) and B(M1)/B(E2) in-band values of the odd-parity bands in ^{110,112}Ru as a function of rotational frequency. Within the present approach both are equal and given by the TAC calculations.

The TAC calculations give a γ-deformation of 22° with the same moment of inertia and similar energy relative to the ground state as bands 4, 5 and 6, 7 in the experimental data. The inband ratios B(M1)/B(E2) are also well described up to $\omega=0.3$ MeV/$\hbar$. The TAC solution has a tilt angle θ that changes rapidly from 0° at $\omega=0.10$ MeV/$\hbar$ toward 60° at $\omega=0.30$ MeV/$\hbar$. The second tilt angle remains at $\varphi=0°$, which indicates that the con-

figuration does not develop static chirality.

We find a low-lying RPA phonon at an excitation energy of 300 keV, which we associate with bands 6, 7 in ^{110}Ru. It has about 1$\hbar$ less aligned angular momentum than the zero phonon state, which is in agreement with the data. As seen in Fig. 13, the TAC + RPA one-phonon energy agrees very well with the distance between the routhians of bands 6, 7 and 4, 5 in ^{110}Ru. Using the method described in Ref. [40], we analyzed the microscopic structure of the RPA solution. We found that it represents a collective motion in the orientation variables θ and φ. The oscillations of the deformation parameters are weak. Hence, the RPA calulations confirm the interpretation as a chiral vibration. Also the RPA values for the interband M1 and E2 transitions are very small, and are consistent with our experimental intensity upper limits for these weak transitions, to further support our interpretation.

To see if band 4, 5 can be interpreted as an alternative neutron configuration, the TAC equations were solved for the second lowest odd-parity, two-quasi-neutron configuration. In Fig. 13 we can see that this configuration has similar energy and moment of inertia as the lower configuration, but has very different $B(\mathrm{M1})/B(\mathrm{E2})$ ratios and is an unlikely candidate for the interpretation of this band. The TAC results are consistent with the additional calculations in the framework of the triaxial-rotor-plus-two-quasi-neutron model, which give substantially different $B(\mathrm{M1})/B(\mathrm{E2})$ ratios for the lowest neutron configurations. It is clear that the doublet bands in ^{110}Ru make the best example of a soft chiral vibration.

In ^{112}Ru, the bands 7, 6 cross bands 4, 5, while both bands stay very close together (see Fig. 8(b)). Ref. [40] demonstrated chiral instability, where RPA breaks down. Thus a direct comparison of the ^{112}Ru data with our TAC+RPA solution is inappropriate. At this point, we interprete the crossing of the bands as a signal of chiral instability. A large amplitude description of the chiral motion is needed and such is in progress[42].

1.3 Concluding remarks for Section 1

^{110,112}Ru and ^{108}Mo fulfill the characteristic conditions for generating chirality, and all the fingerprints for chiral doublets are identified in the two sets of $\Delta I=1$ odd-parity doublet bands observed in the isotopes. The partner levels of the doublet bands in ^{110,112}Ru and ^{108}Mo have very similar electromagnetic properties: their $B(\mathrm{E2})/B(\mathrm{M1})$ ratios are very similar. Their energy staggering parameter $S(I)$ values are nearly equal and constant with spin. They are the most nearly degenerate in energy of any of the proposed chiral bands. These data and the fact that the two bands cross and the interband ratios are weak suggest these bands are a soft chiral vibration, i. e. a slow motion of the angular momentum relative to the three-axial nuclear shape between left-handed and right-handed geometries, where it resides for most of the time. These features can be explained by tilted axis cranking calculations, which are extended by RPA calculations, which describe the slow vibrational motion but a simple geometrical explanation is not apparent. These doublets are zero-and one-phonon chiral vibration bands built on a $\nu h_{11/2}\otimes(d_{5/2}g_{7/2})^{-1}$ configuration. The γ softness in ^{108}Ru may have disturbed the chirality in the nucleus, and a likely evolution of chirality from γ soft ^{108}Ru to triaxial ^{110,112}Ru is proposed.

References(Section 1):

[1] Hamilton J H, Ramayya A V, Zhu S J, *et al*. Prog Part Nucl Phys, 1995, **35**: 635.

[2] Zhang C T, Bhattacharyya P, Daly P J, *et al*. Phys Rev Lett, 1996, **77**: 3743.

[3] Baxter A M, Khoo T L, Bleich M E, *et al*. Nucl Inst and Meth, 1992, **A317**: 101.

[4] Radford D C. Nucl Inst and Meth, 1995, **A317**: 297, also cf. his website http://radware.phy.ornl.gov/.

[5] Hamilton J H, TerAkopian G M, Oganessian Y T, *et al*.

Phys Rep, 1996, **264**: 215.
[6] Wu S C, Donangelo R, Rasmussen J O, *et al*. Phys Rev, 2000, **C62**: 041601.
[7] Daniel A V, Goodin C, Li K, *et al*. Nucl Instr and Meth, 2007, **B262**: 399.
[8] Frauendorf S, Meng J. Nucl Phys, 1997, **A617**: 131.
[9] Frauendorf S. Rev Mod Phys, 2001, **73**: 463.
[10] Koike T, Starosta K, Hamamoto I, *et al*. Phys Rev Lett, 2004, **93**: 172502.
[11] Vaman C, Fossan D B, Koike T, *et al*. Phys Rev Lett, 2004, **92**: 032501.
[12] Starosta K, Koike T, Chiara C J, *et al*. Phys Rev Lett, 2001, **86**: 971.
[13] Dimitrov V I, Frauendorf S. Proc. Third Int. Conf. Fission and Properties of Neutron-rich Nuclei. In: Hamilton J H ed. Singapore: World Scientific, 2003, 93.
[14] Hecht A A, Beausang C W, Zyromski K E, *et al*. Phys Rev, 2001, **C63**: 051302.
[15] Starosta K, Chiara C J, Fossan D B, *et al*. Phys Rev, 2001, **C63**: 061304.
[16] Starosta K, Chiara C J, Fossan D B, *et al*. Phys Rev, 2002, **C65**: 044328.
[17] Mergel E, Petrache C M, Lo Bianco G, *et al*. Eur Phys J, 2002, **A15**: 417.
[18] Zhu S, Garg U, Nayak B K, *et al*. Phys Rev Lett, 2003, **91**: 132501.
[19] Grodner E, Srebrny J, Pasternak A A, *et al*. Phys Rev Lett, 2000, **97**: 172501.
[20] Koike T, Starosta K, Chiara C J, *et al*. Phys Rev, 2003, **C67**: 044319.
[21] Timar J, Joshi P, Starosta K, *et al*. Phys Lett, 2004, **B598**: 178.
[22] Joshi P, Jenkins D G, Raddon P M, *et al*. Phys Lett, 2004, **B595**: 135.
[23] Timar J, Vaman C, Starosta K, *et al*. Phys Rev, 2006, **C73**: 011301(R).
[24] Joshi P, Wilkinson A R, Koike T, *et al*. Eur Phys J, 2005, **A24**: 23.
[25] Zhu S J, Hamilton J H, Ramayya A V, *et al*. Eur Phys J, 2005, **A25**: 459.
[26] Joshi P, Carpenter M P, Fossan D B, *et al*. Phys Rev Lett, 2007, **98**: 102501.
[27] Petrache C M, Hagemann G B, Hamamoto I, *et al*. Phys Rev Lett, 2006, **96**: 112502.
[28] Tonev D, de Angelis G, Brant S, *et al*. Phys Rev, 2007, **C76**: 044313.
[29] Mukhopadhyay S, Almehed D, Garg U, *et al*. Phys Rev Lett, 2007, **99**: 172501.
[30] Luo Y X, Zhu S J, Hamilton J H, *et al*. Phys Lett, 2009, **B670**: 307.
[31] Luo Y X, Zhu S J, Hamilton J H, *et al*. Intern Jour of Moder Phys, 2009, **E18**(8): 1697.
[32] Aysto J, Jauho P P, Janas Z, *et al*. Nucl Phy, 1990, **A515**: 365.
[33] Luo Y X, Wu S C, Gilat J, *et al*. Phys Rev, 2004, **C69**: 024315.
[34] Luo Y X, Rasmussen J O, Hamilton J H, *et al*. Phys Rev, 2004, **C70**: 044310.
[35] Luo Y X, Rasmussen J O, Stefanescu I, *et al*. J Phys, 2005, **G31**: 1303.
[36] Luo Y X, Hamilton J H, Rasmussen J O, *et al*. Phys Rev, 2006, **C74**: 024308.
[37] Möller P, Bengtsson R, Carlsson B G, *et al*. Phys Rev Lett, 2006, **93**: 162502.
[38] Stefanescu I, Gelberg A, Jolie J, *et al*. Nucl Phys, 2007, **789**: 125.
[39] Zhu S J, Luo Y X, Hamilton J H, *et al*. Intern Jour of Moder Phys, 2009, **E18**(8): 1717.
[40] Almehed D, Frauendorf S. Submitted Phys Rev C, arXiv: 0709: 0969
[41] Baranger M, Kumar K. Nuc Phys, 1968, **A110**: 490.
[42] Almehed A, Frauendorf S. to be published.

2 High-spin Nuclear Structure in the Vicinity of Doubly-magic ^{132}Sn: Systematic Search and Studies of Neutron-rich $N=83$ Isotonic Chain with Few Valence Protons Outside the $Z=50$ Major Shell

2.1 Introduction

Structure of nuclei in the vicinity of doubly-magic ^{132}Sn ($Z=50$, $N=82$) has been of special interest. Important information such as nucleon-nucleon interactions can be extracted from investigations in this region. The nuclei near the $N=82$ closed shell span a broad range of Z. A straightforward and important question is "To what extent is the spherical shell model (SSM) valid for nuclei near $N=82$?" The answers to these questions provide stringent tests of the basic ingredients of the spherical shell model calculations. With one va-

lence neutron outside the $N=82$ closed shell and few valence protons beyond the $Z=50$ closed shell, the $N=83$ isotones' yrast spectroscopy is of significance for the information about empirical proton-neutron and proton-proton interactions. It was pointed out in Ref. [1] that the orbitals above and below the corresponding gap of ^{132}Sn and ^{208}Pb region, respectively, are similarly ordered. For every single particle state in the ^{132}Sn region there is its counterpart around ^{208}Pb, the latter being with the same radial quantum number n, and one unit larger in angular momenta l and j. The similarity of structure between the ^{132}Sn and ^{208}Pb region suggests that the well-studied ^{208}Pb region may provide important information like nucleon-nucleon interactions for the calculations in ^{132}Sn region.

The β^- decay from fission[2] was used to populate low spin states of the $N=83$ isotones. A yrast and near yrast level scheme of ^{139}Ba extending to an excitation of 2743.4 keV was established via ^{136}Xe (α, n) reaction[3]. About ten years ago preliminary high-spin yrast and near-yrast spectroscopy of the $N=83$ isotonic chain was studied in ^{134}Sb ($Z=51$), ^{135}Te ($Z=52$), ^{136}I ($Z=53$)[4], and ^{137}Xe ($Z=54$)[5] at Gammasphere and Eurogam II with spontaneous fission sources.

Using our 2000's high statistics, high quality triple coincidence data (see the previous subsection 1.2.2), a systematic investigation along the $N=83$ isotonic chain was performed. The detailed studies of high-spin yrast and near-yrast spectroscopy of the $N=83$ isotonic chain were extended to ^{138}Cs ($Z=55$)[6] which had long been missing, and the level schemes established before in ^{134}Sb ($Z=51$), ^{135}Te ($Z=52$), ^{136}I ($Z=53$)[4], ^{137}Xe ($Z=54$)[5], and ^{139}Ba ($Z=56$)[3] were considerably extended and expanded[7—9]. An isomer state was identified in ^{136}I by Urban et al.[10]. This section will review the new insights from the yrast and near-yrast spectroscopy of the $N=83$ isotones based on the new level schemes established by our collaboration at Gammasphere.

2.2 Level structure of the $N=83$ isotones: ^{135}Te ($Z=52$), ^{136}I ($Z=53$), ^{137}Xe ($Z=54$), ^{138}Cs ($Z=55$) and ^{139}Ba ($Z=56$)

2.2.1 Extensively extended and expanded new level scheme of ^{135}Te ($Z=52$) and the first observation of tilted rotation (magnetic rotation, shears band) in the vicinity of doubly-magic ^{132}Sn

An extensively extended and expanded level scheme of ^{135}Te was established by our collaboration[8] (see Fig. 1), while a similar but less complete one was published by Fornal et al.[11]. J^π of

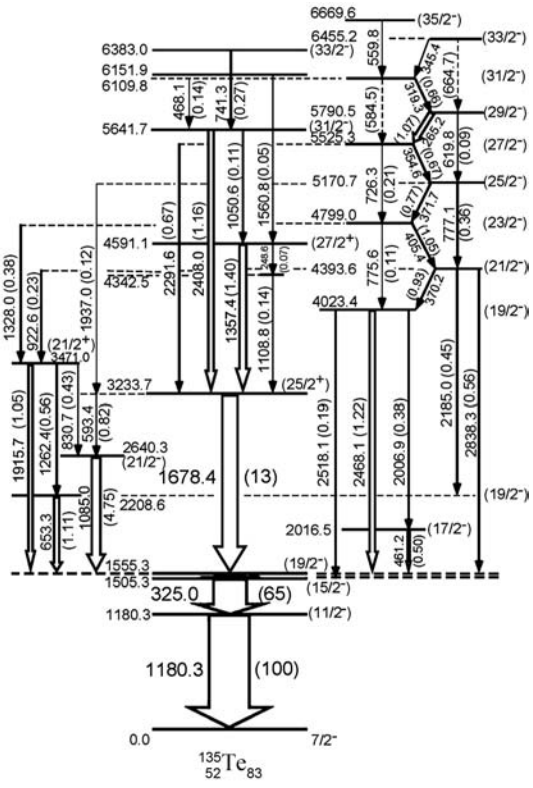

Fig. 1 Our extended and expanded new level scheme of ^{135}Te[8]. Note the high-lying regular spaced $\Delta I=1$ band built on several irregular high-energy transitions, and the enhanced 2408.0—1678.4 keV stretched E3 cascade.

$25/2^+$, $27/2^+$ and $31/2^-$ were assigned, respectively, to the 3233.7, 4591.1 and 5641.7 keV levels and confirmed by SM calculations[11], and enhanced cascading stretched E3 transitions of 1678.4 and 2408.0 keV were identified. Based on shell model calculations and comparison of the level pat-

tern with that of ^{134}Te, single proton-neutron excitations, $\pi g_{7/2}^2 \nu f_{7/2}$, $\pi g_{7/2} d_{5/2} \nu f_{7/2}$, $\pi g_{7/2} h_{11/2} \nu f_{7/2}$, and $\pi g_{7/2} h_{11/2} \nu i_{13/2}$ etc., are assigned to levels in ^{135}Te.

However, the particular interesting observations in ^{135}Te are the high-lying regular sequence at 4023.4—6669.6 keV excitations above several irregular high-energy transitions. Ref. [12] did not report a complete sequence with linkings and cross-overs, and interpreted the levels as core excitations ($\pi g_{7/2}^2 \nu f_{7/2}^2 h_{11/2}^{-1}$).

Our special attention was paid to the identifications and measurements of the four weak E2 cross-overs and six M1 linking transitions in the high-lying regular spaced $\Delta I=1$ band in ^{135}Te (see Fig. 1). J^π of $(19/2^-)$, $(21/2^-)\cdots(33/2^-)$ were assigned to this newly identified intriguing band. A regular spacing $\Delta I=1$ band with strong M1 linkings and weak E2 cross-overs built on several irregular high-energy transitions was thus identified in ^{135}Te (see Fig. 1). This $\Delta I=1$ regular band, which is very similar to the observations in Pb isotopes, was interpreted as a good example of tilted rotation in a weakly deformed nucleus[8].

In Pb isotopes, regular spacing $\Delta I=1$ bands built on irregular transitions were measured to have very large B(M1) and substantial moments of inertia[13]. These bands in Pb isotopes were interpreted to be tilted rotations (magnetic rotations). In these bands a few high-j orbitals generate j, and high-j particle (formed by proton excitation into $h_{9/2}$ and $i_{13/2}$ orbitals) and high-j hole (formed by neutron-excitation in the $i_{13/2}$ sub-shell) have a large angle, with the j gradually aligning J to form a band. Such high-spin particle/high-spin hole states have a transverse magnetic dipole moment with large components perpendicular to the J. The magnetic moments rotate about J to create enhanced M1 transitions[14, 15].

The high-lying regular spacing $\Delta I=1$ band identified in ^{135}Te was interpreted as a tilted band based on the following arguments: (A) The observation of a regular spaced $\Delta I=1$ band with enhanced M1; (B) This band is built on irregular high-energy transitions in a very weakly-deformed nucleus. The tilted band proposed in ^{135}Te is interpreted as coupling of a high-spin particle to a high-spin hole excitation: The high-spin hole —— the $h_{11/2}$ neutron hole from neutron excitation has its angular momentum vector tilted but mainly along the long axis of the weakly deformed core, while the high-spin particle pairs —— proton and neutron particle pairs beyond the closed shell contribute to an angular momentum vector tilted but mainly perpendicular to the long axis. These two angular momentum vectors will have considerably different g factors, giving rise to strong M1 transition.

This is the first observation of tilted rotation (magnetic rotation) in the vicinity of doubly-magic ^{132}Sn.

2.2.2 New level scheme of ^{136}I ($Z=53$) and the tentative interpretation for its level structure

By using our high-statistics triple-coincidence data the yrast and near-yrast level scheme of ^{136}I[7] was considerably extended from ~ 4.0 MeV[4] to 5.433 MeV with 21 new levels identified (see Fig. 2). In the level scheme the excitation energy of the 7^- level is set to be zero. Urban et al. have reported a $T_{1/2}=47$ s isomer which is 42.6 keV below the 7^- level[10].

The newly observed transitions are too weak to make angular correlation measurements. The assignments for reported levels of ^{136}I follow those in Ref. [4], and the spin/parity is tentatively assigned to the newly identified levels based on level systematics. 17^- is tentatively assigned to the new 5114.9 keV level based on the analogy of level pattern to ^{135}Te.

The shell-model calculations in Ref. [4] suggested the interpretation of the ^{136}I levels up to 1615.6 keV as members of the $\pi g_{7/2}^3 \nu f_{7/2}$ and $\pi g_{7/2}^2 d_{5/2} \nu f_{7/2}$ multiplets, and levels around 2.9 MeV as $\pi g_{7/2}^2 h_{11/2} \nu f_{7/2}$. We feel it is reasonable to

tentatively assign $(\pi g_{7/2}^2 h_{11/2} \nu i_{13/2})_{17^-}$ to the level of 5114.9 keV of ^{136}I we observed, so enhanced cascading stretched E3 transitions, 2097.7 keV — 1644.8 keV, are likely observed in ^{136}I, which is similar to those in ^{135}Te.

Urban et al.[10] interpreted the 47 s isomer (6^-) below the 7^- level as $(\pi g_{7/2}^2 d_{5/2} \nu f_{7/2})_{6^-}$. The assignment was supported by model calculations of the SMPN(400) set of two body matrix, in which the position of the $d_{5/2}$ orbital was lowered by 400 keV. They also suggested that the change in the position of the $d_{5/2}$ orbital is related to a local effect in the region of the ^{132}Sn core, which is of theoretical interest.

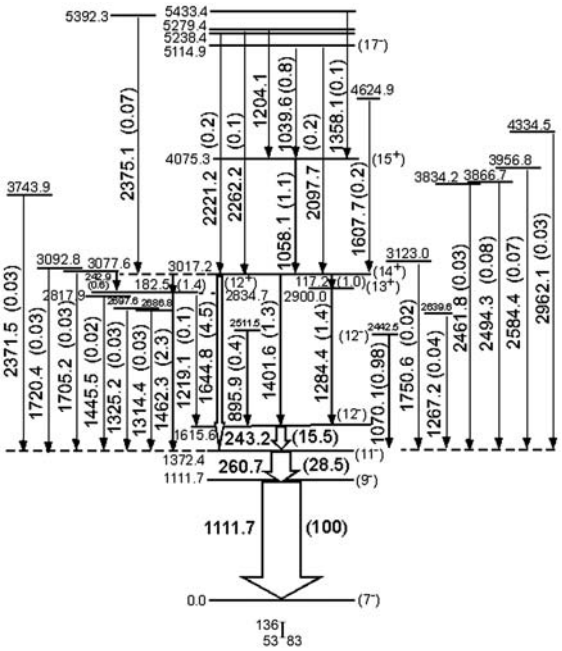

Fig. 2 Our extended and expanded new level scheme of ^{136}I. The excitation of the 7^- level is set to be zero. A $T_{1/2}$ = 47 s isomer of 6^- and 42.6 keV below the 7^- level was recently reported in Ref. [10]. Like the case in ^{135}Te, enhanced stretched E3 cascade, 2097.7 — 1644.8 keV, is likely identified in ^{136}I. See text.

2.2.3 New level scheme of ^{137}Xe (Z=54) and the tentative interpretation for its level structure

The previously reported level scheme of ^{137}Xe[5] was extended from an excitation energy of ~ 4.5 MeV to 6.690 MeV with 11 new levels identified (see Fig. 3)[7]. Spin-parity assignments were made for ^{137}Xe earlier[5] in which the assignments were made by means of angular correlation and linear polarization measurements; and $39/2^-$ is tentatively assigned to the new 6689.8 keV level in view of the similar level pattern and spacing to those of ^{135}Te. Enhanced stretched E3 cascade, 2001.7 — 1395.9 keV, is thus likely identified, which is similar to those in ^{135}Te and ^{136}I.

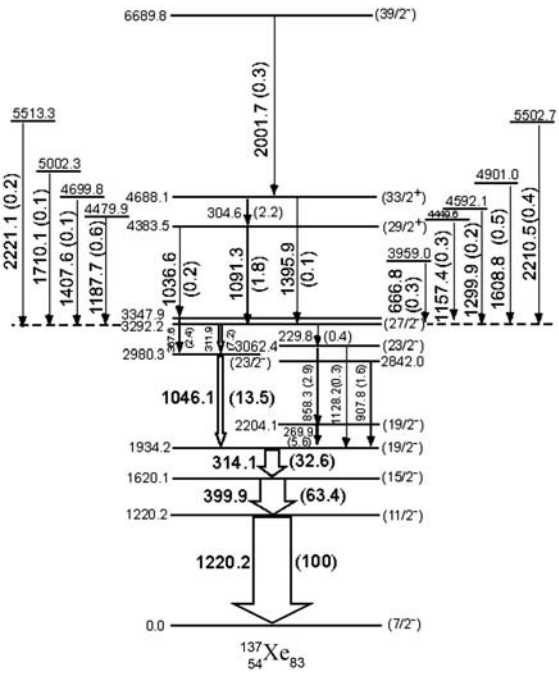

Fig. 3 Our extended and expanded new level scheme of ^{137}Xe[7]. Enhanced stretched E3 cascade, 2001.7 — 1395.9 keV, is likely identified.

The level structure of ^{137}Xe is attributed to coupling between the configurations of ^{136}Xe with an additional $f_{7/2}$ valence neutron, the latter being assigned by means of shell model calculations as four valence protons with related single particle excitations ($\pi g_{7/2}^4$, $\pi g_{7/2}^3 d_{5/2}$ and $\pi g_{7/2}^3 h_{11/2}$)[5]. The newly identified 6689.8 keV level in ^{137}Xe is assumed to come from $(\pi g_{7/2}^3 h_{11/2}\ \nu i_{13/2})_{39/2^-}$.

2.2.4 First observation of the high-spin level scheme of ^{138}Cs (Z=55) and the shell-model calculations

In the N = 83 isotonic chain adjacent to the doubly magic ^{132}Sn, the important member ^{138}Cs (Z=55) had long been missing. Through intensive

search by using our high statistics and high quality triple-coincidence data at Gammasphere, its yrast and near-yrast level scheme was observed for the first time(Fig. 4)[6]. The spin/parity and configurations were assigned to the levels of ^{138}Cs based on internal conversion coefficient (ICC) measurements of the low-energy transitions, angular correlation measurements, shell-model calculations and level systematics. Unlike the cases in ^{135}Te (Z=52), ^{136}I (Z=53) and ^{137}Xe (Z=54), no enhanced stretched E3 cascading transitions are identified in ^{138}Cs.

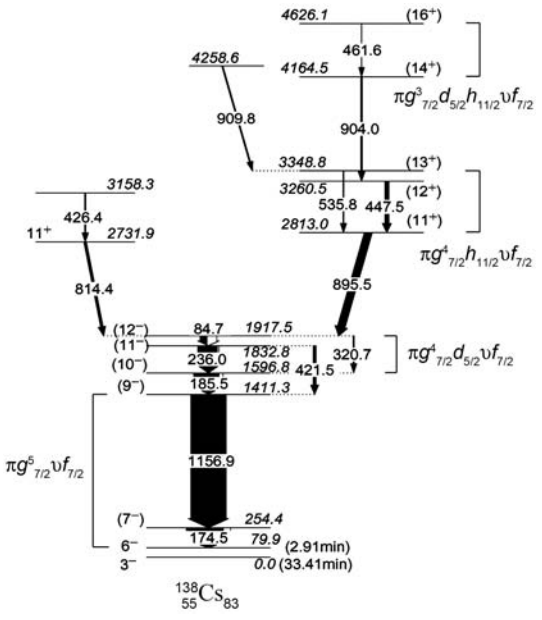

Fig. 4 High-spin level scheme of ^{138}Cs identified for the first time by our collaboration[6]. The levels are built on the 6^- isomeric state. The leading components of the configurations assigned by shell model calculations are also displayed in the figure.

In the shell-model (SM) calculations for ^{138}Cs it was assumed that the valence protons outside the ^{132}Sn closed core occupy the five single-particle (SP) orbits of the 50—82 shell, while for the neutrons the model space includes the six orbits of the 82—126 shell. A shell model Hamiltonian was employed with the single-particle energies taken from experiment and the two-body effective interaction derived from the CD-Bonn free nucleon-nucleon potential[16]. The same Hamiltonian was used in recent studies in this nuclear region(e. g. Ref. 17). It should be noted that the SM calculations are completely free from the adjustable parameters.

Table 1 shows the results of the SM calculations for ^{138}Cs and the leading components and their percentages of the total theoretical wave function. It can be seen in the table that good agreements are obtained between experimental and theoretical excitations, and the configuration mixing in

Table 1 Comparison of experimental (E_{ex}) and calculated (E_{th}) level energies of ^{138}Cs, and the deviations between them. The excitation energies are relative to the(6^-) level

I^π	E_{ex} /MeV	E_{th} /MeV	$\Delta=E_{th}-E_{ex}$ /MeV	Leading component	Percentage
6^-	0.0	0.0	0.0	$\pi g^5_{7/2}\nu f_{7/2}$	46
7^-	0.17	0.15	−0.02	$\pi g^5_{7/2}\nu f_{7/2}$	41
9^-	1.33	1.55	0.22	$\pi g^5_{7/2}\nu f_{7/2}$	51
10^-	1.52	1.75	0.23	$\pi g^4_{7/2}d_{5/2}\nu f_{7/2}$	80
11^-	1.75	1.89	0.14	$\pi g^4_{7/2}d_{5/2}\nu f_{7/2}$	57
12^-	1.84	1.98	0.14	$\pi g^4_{7/2}d_{5/2}\nu f_{7/2}$	77
11^+	2.73	2.79	0.06	$\pi g^4_{7/2}h_{11/2}\nu f_{7/2}$	61
12^+	3.18	3.25	0.07	$\pi g^4_{7/2}h_{11/2}\nu f_{7/2}$	61
13^+	3.27	3.33	0.06	$\pi g^4_{7/2}h_{11/2}\nu f_{7/2}$	63
14^+	4.08	3.80	−0.28	$\pi g^3_{7/2}d_{5/2}h_{11/2}\nu f_{7/2}$	81
16^+	4.55	4.43	0.08	$\pi g^3_{7/2}d_{5/2}h_{11/2}\nu f_{7/2}$	79

^{138}Cs is extensive. The coupling between the $g_{7/2}$ valence protons and the $f_{7/2}$ neutron, $\pi g^5_{7/2}\nu f_{7/2}$, is assigned to the first excitations, (6^-), (7^-) and (9^-) levels. The $g_{7/2}\rightarrow d_{5/2}$ proton excitation coupled to the $f_{7/2}$ neutron, $\pi g^4_{7/2}d_{5/2}\nu f_{7/2}$, is assigned to the ($10^-$), ($11^-$) and ($12^-$) levels. The coupling of the $f_{7/2}$ neutron with the $g_{7/2}\rightarrow h_{11/2}$ and $(g_{7/2})^2\rightarrow d_{5/2}\,h_{11/2}$ odd-parity proton excitations, $\pi g^4_{7/2}h_{11/2}\,\nu f_{7/2}$ and $\pi g^3_{7/2}\,\mathrm{d}_{5/2}\,h_{11/2}\,\nu f_{7/2}$, fit well the first three even-parity levels (11^+), (12^+), (13^+), and the following (14^+) and (16^+), respectively. The comparison between experiment and SM calculations reveal significant contributions by the couplings between the excitations of the few

valence protons outside the $Z=50$ major shell closure with the $f_{7/2}$ neutron outside the $N=82$ major shell closure.

Fig. 5 displays the yrast excitations of Cs isotopes near the $N=82$ neutron major shell closure. The level spacing of both the even-neutron (upper) and the odd-neutron (lower) Cs isotopes exhibit strong shell effects of the $N=82$ major shell. The low-lying levels excited in the odd-neutron Cs isotopes may imply the role of the coupling between the odd-neutron outside the $N=82$ shell closure with the few valence protons outside the $Z=50$ shell closure.

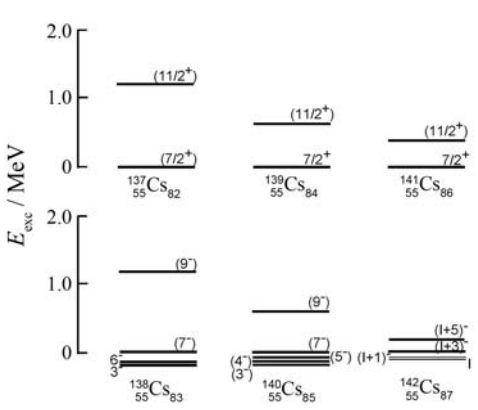

Fig. 5 Yrast states of Cs isotopes. Data are taken from Ref. [6] and Refs. [18—21]. Shell effects of the $N=82$ major shell are clearly seen as the evolution of the level spacings with changing neutron number.

Fig. 6 shows the yrast excitations of the $N=82$ and $N=83$ isotones with three and five protons outside the $Z=50$ proton major shell closure. A similarity is seen in the $N=82$ isotones. However, while a similar cascade pattern is observed in $N=83$ isotones, one more yrast state, the (10^-) state, was identified in ^{138}Cs. It should be noted that the interposition of this (10^-) state between the (9^-) and (11^-) levels in ^{138}Cs is not seen in ^{136}I ($Z=53$, $N=83$)(see Fig. 6), and not in ^{137}Cs ($N=82$) either. These observations and the SM calculations may imply that while the overall structure in this nuclear region can be interpreted by the coupling between the $f_{7/2}$ valence neutron outside the $N=82$ major shell closure with the excitations of the few valence protons outside the $Z=50$ major shell closure, one should note the important role of the coupling between the $f_{7/2}$ valence neutron with the fifth valence proton outside the shell closure.

As mentioned in the previous 2. 2. 2 subsection, the 47 s isomer (6^-) below the 7^- level in ^{136}I was interpreted as $(\pi g_{7/2}^2 d_{5/2}\nu f_{7/2})_{6^-}$ by Urban et al.[10]. However, in our SM calculations this (6^-) in ^{138}Cs was interpreted as $\pi g_{7/2}^5\nu f_{7/2}$ with no $g_{7/2}\rightarrow d_{5/2}$ proton excitation, and in which the lowest (6^-) level in ^{136}I was assigned the same $\pi g_{7/2}^3\nu f_{7/2}$ dominant configuration[22]. Note that our calculations of ^{136}I also predicted a 10^- state with $\pi g_{7/2}^3\nu f_{7/2}$ dominant configuration at about the same E_{th} as that of ^{138}Cs, which was, however, not observed in ^{136}I (see Fig. 2). Further theoretical studies are needed to throw light upon this question.

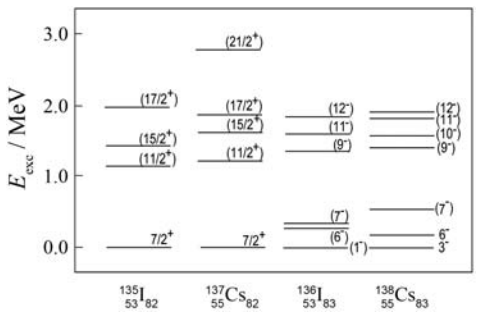

Fig. 6 Yrast states of the $N=82$ and $N=83$ isotones. Similarity is seen in $N=82$ isotones. In $N=83$ isotones, although one can see a similar cascade pattern, an state interposed between the (9^-) and (11^-) level is observed in ^{138}Cs, but not in ^{136}I, implying the important role played by the coupling between the valence $f_{7/2}$ neutron with the fifth valence proton.

The variations of the excitation energies of the $11/2^+$ state in even-N Cs isotopes versus the excitations of the first 2^+ state in the corresponding even-even Xe core are shown in Fig. 7. They change very rapidly in the region of $N=82$ major shell with an almost linear relationship. The $N=83$ Cs isotone, ^{138}Cs, is also shown in the figure by assuming that the corresponding 9^- state can be attributed to the coupling between the lowest yrast

excitation of the even-even core ^{136}Xe with one $g_{7/2}$ valence proton and one $f_{7/2}$ neutron. For ^{138}Cs, the coupling does not significantly reduce the excitation energy of the corresponding 9^- state.

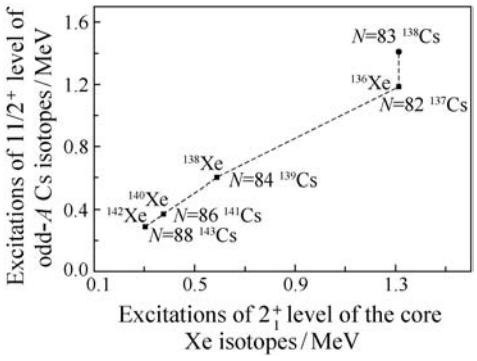

Fig. 7 The E_{ex} of the $11/2^+$ state in even-N Cs isotopes plotted against the E_{ex} of the $(2^+)_1$ in even-even Xe core. ^{138}Cs is also shown in the figure.

2.2.5 New level scheme of ^{139}Ba ($Z=56$) and the discussion of its nuclear structure

High spin states of ^{139}Ba were proposed by our collaboration [8] by fission γs detection at Gammasphere (Fig. 8). The level scheme reported in Ref. [3] was considerably extended and expanded from excitation of 2091.7 keV to 4956.7 keV with 11 new transitions observed. In Ref. [3] the levels up to 1976.6 keV were interpreted in terms of particle-core coupling (PCC) approach, in which the coupling of the $f_{7/2}$ neutron to the low-lying even-parity states in the core ^{138}Ba form the states in ^{139}Ba up to the 1976.6 keV level, which was assigned as $(17/2^-)$. Based on the previous assignments to the lower-lying states, spins, parities and configurations were tentatively assigned to the new levels of ^{139}Ba in terms of particle-hole coupling[8]. In view of the six protons in the $g_{7/2}$ subshell in ^{139}Ba, the 2091.7 keV state was interpreted as $(\pi g_{7/2}^{-2}\nu f_{7/2})_{(19/2^-)}$, the new levels at and above the 3122.8 keV excitation in ^{139}Ba (see Fig. 8) were tentatively interpreted as excitation of the two $g_{7/2}$ proton holes coupled to the $f_{7/2}$ neutron, $(\pi g_{7/2}^{-3} d_{5/2}\nu f_{7/2})_{(21/2^-,\,25/2^-,\,29/2^-,\,31/2^-)}$ [7, 8].

The level structure of ^{139}Ba exhibits remarkable differences in comparison with that of ^{135}Te, ^{136}I and ^{137}Xe. Unlike the cases of ^{135}Te, ^{136}I and ^{137}Xe, no enhanced stretched E3 cascade is observed in ^{139}Ba (Fig. 8). However, similar level patterns are seen in ^{139}Ba and ^{138}Cs. Like the case of ^{138}Cs, a yrast $(17/2^-)$ level has interposed itself between the $(15/2^-)$ and $(19/2^-)$ levels in ^{139}Ba, and in both the ^{139}Ba and ^{138}Cs one does not see the E3 cascade. This interesting diversity may be partly attributed to the difference of particle-particle coupling in ^{135}Te (two valence protons), ^{136}I (three protons), and ^{137}Xe (four protons), and particle-hole coupling in ^{139}Ba (a pair of proton-holes), respectively.

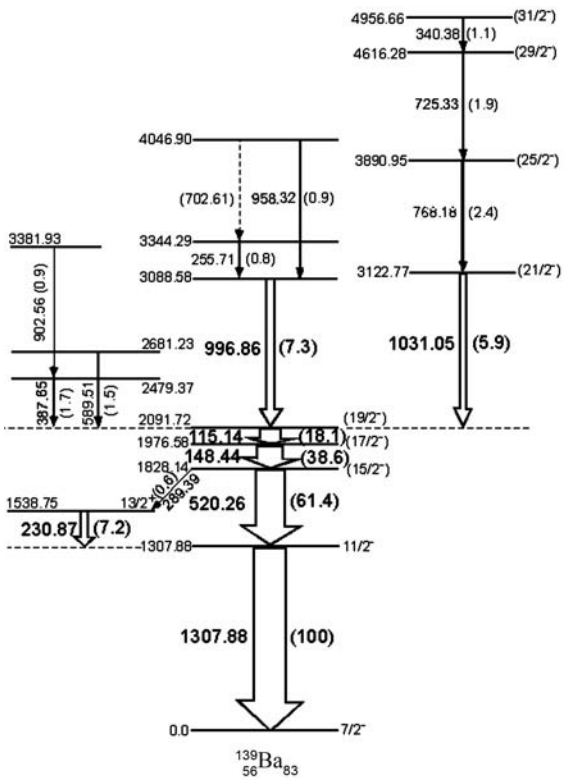

Fig. 8 New level scheme of ^{139}Ba extended and expanded by detecting fission γs by Gammasphere.

In Ref. [3] the PCC model calculations did not reproduce the level at 2091.7 keV. So the interposition of the yrast $(17/2^-)$ level was not explained. In Ref. [8] of our collaboration this interposition was qualitatively explained by particle-hole coupling. Recall that the odd-odd nuclei near double-closed-shell particle-particle or hole-hole nuclei

have a multiplet splitting pattern that makes the stretched (maximum spin) and antistretched (minimum spin) multiplet members lower in energy than intermediate-spin members. For the particle-hole cases the lowest energy member is usually of spin one less than the stretched maximum. Thus one would expect that the particle-hole coupling in ^{139}Ba would have the $(17/2^-)$ lying below $(19/2^-)$ in the multiplet of $(\pi g_{7/2}^{-2})_6 \nu f_{7/2}$. In other words, the particle-hole coupling in ^{139}Ba case has lowered states of spin one less than that of the fully stretched configuration, which explains why the $(17/2^-)$ level interposes itself between $(15/2^-)$ and $(19/2^-)$ levels in ^{139}Ba. The interposed level effectively "short circuits" the possible analogous stretched E3 transitions with lower multipolarity transitions in the nucleus.

The interposed yrast (10^-) level and the absence of a stretched E3 cascade in ^{138}Cs (see the previous section) are likely analogous to the interposition of the yrast $(17/2^-)$ level and the non-observation of a stretched E3 cascade in ^{139}Ba, and can probably be explained in a similar way.

2.3 Resemblance of spectroscopy and the counterparts observed between the $N=83$ isotones in ^{132}Sn region and the corresponding $N=127$ isotones in ^{208}Pb region

Based on the new level schemes proposed and interpreted for the $N=83$ isotonic chain, a resemblance of spectroscopy and the counterparts are observed between the yrast three-particle states in ^{135}Te and ^{211}Po, and between the possible yrast five-particle states in ^{137}Xe and ^{213}Rn (see Fig. 9, and Refs. [8, 11, 23]), and also in ^{136}I and ^{212}At. In Fig. 9 similar level patterns and spectacular stretched cascading E3 transitions are seen in each pair of nuclei. One sees the possibility that the well-studied ^{208}Pb region may provide important information like nucleon-nucleon interactions for the calculations in corresponding nuclei in ^{132}Sn region.

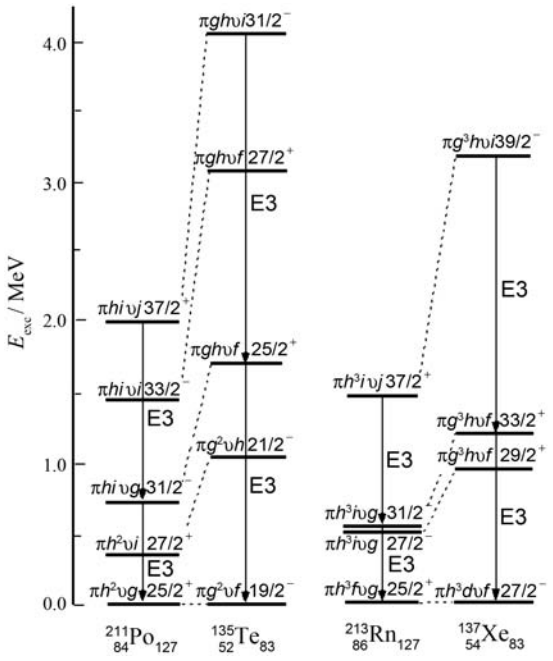

Fig. 9 Comparison of yrast three-particle states in ^{135}Te and ^{211}Po, and of the possible yrast five-particle states in ^{137}Xe and ^{213}Rn[23]. See text.

2.4 Concluding remarks for Section 2

By using the high statistics triple-coincidence fission γ data at Gammasphere, high-spin yrast and near-yrast level schemes of the $N=83$ isotones ^{135}Te, ^{136}I, ^{137}Xe and ^{139}Ba were considerably extended and expanded, and that of ^{138}Cs was identified for the first time. Spin/parity and configurations were assigned based on ICC measurements, angular correlation measurements, shell model (SM) calculations and level systematics. The detailed studies of yrast and near-yrast spectroscopy of the $N=83$ isotonic chain were extended to ^{138}Cs ($Z=55$) which had long been missing. The level schemes of the $N=83$ isotonic chain and the SM calculations indicated the key role played by the coupling of the excitations of the few valence protons ($g_{7/2}$) outside the $Z=50$ major shell closure and the valence neutron ($f_{7/2}$) outside the $N=82$ major shell closure. Strong shell effects of the $N=82$ major shell is seen in the level evolution in ^{137,138,139,140,142}Cs. While similar level patterns were observed in $N=82$ isotones ^{137}Cs and ^{135}I, differences were seen in $N=83$ isotones ^{138}Cs and

^{136}I, and in isotopes ^{138}Cs and ^{137}Cs, implying the important role played by the coupling between the valence $f_{7/2}$ neutron with the fifth valence proton. The spectacular stretched E3 cascading transitions were seen in ^{135}Te, ^{136}I and ^{137}Xe, but were not found in ^{138}Cs and ^{139}Ba. Interposition of the yrast $(10^-)_1$ level in ^{138}Cs and of the yrast $(17/2^-)_1$ in ^{139}Ba were observed in the two $N=83$ isotones. The level interposition and the lack of the stretched E3 cascading transition in ^{139}Ba and ^{138}Cs may be qualitatively explained by the particle-hole coupling approach. Tilted rotation(magnetic rotation) was observed in ^{135}Te, which is the first observation of such a shears band in the vicinity of the doubly-magic ^{132}Sn. The resemblance of spectroscopy and counterparts were observed between the three-particle states in ^{135}Te and ^{211}Po, and between the five-particle states in ^{137}Xe and ^{213}Rn.

References(Section 2):

[1] Blomqvist J. In Proceedings of the 4th Inter Conf on Nucl Far From Stability, Helsingoer: Denmark, 1981, 536.

[2] Firestone R B, Shirley V S. Table of Isotopes, 8th ed, New York: Wiley, 1996.

[3] Prade H, Enghardt W, Dioszegi I, *et al*. Nucl Phys, 1987, **A472**: 381.

[4] Bhattacharyya P, Zhang C T, Fornal B, *et al*. Phys Rev, 1997, **C56**: R2363.

[5] Daly P J, Bhattacharyya P, Zhang C T, *et al*. Phys Rev, 1999, **C59**: 3066.

[6] Li K, Luo Y X, Hwang J K, *et al*. Phys Rev, 2007, **C75**: 044314.

[7] Luo Y X, Rasmussen J O, Hamilton J H, *et al*. In Fission and Properties of Neutron-rich Nuclei. In: Hamilton J H, Ramayya, A V, Carter H K. Proceedings of the 3rd International Conference, Sanibel Island, Florida, USA, Singapore: World Scientific, 2003, 310.

[8] Luo Y X, Rasmussen J O, Ramayya A V, *et al*. Phys Rev, 2001, **C64**: 054306-1.

[9] Hwang J K, Ramayya A V, Hamilton J H, *et al*. Phys Rev, 2004, **C69**: 057301.

[10] Urban W, Sarkar M S, Sarkar S, *et al*. Eur Phys J, 2006, **A27**: 257.

[11] Fornal B, Broda R, Krolas W, *et al*. In Proceedings of the International Conference on Nuclear Physics Close to the Barrier, Warszawa, Poland, (June 30, 1998), Acta Physica Polonica, 1999, **B30**(5): 1219.

[12] Fornal B, Broda R, Daly P J, *et al*. Phys Rev, 2001, **C63**: 024322.

[13] Baldsiefen G, Hubel H, Korten W G, *et al*. Nucl Phys, 1944, **A574**: 521.

[14] Frauendorf S. Nucl Phys, 1993, **A557**: 259c; ibid, 2000, **A677**: 115.

[15] Frauendorf S. Z Phys, 1997, **A358**: 153.

[16] Machleidt R. Phys Rev, 2001, **C63**: 024001.

[17] Covello A, Manfredi V R, Azziz N, *et al*. to be published, available online at www. sciencedirect. com.

[18] Liu S H, Hamilton J H, Ramayya A V, *et al*. Phys Rev, 2009, **C80**: 044314.

[19] Luo Y X, Rasmussen J O, Hamition J H, *et al*. Nucl Phys, 2010, **A823**: 1.

[20] Liu S H, Hamilton J H, Ramayya A V, *et al*. Phys Rev, 2010, **C81**: 037302.

[21] Liu S H, Hamiltion J H, Ramayya A V, *et al*. Phys Rev, 2010, **C84**: 057304.

[22] Coraggio L, *et al*. Unpublished.

[23] Stuchbery A E, Dracoulis G D, Byrne A P, *et al*. Nucl Phys, 1988, **A482**: 692.

Gammasphere 上裂变丰中子核核结构若干前沿领域的新进展（Ⅰ：第一和第二部分）*

Y. X. Luo(罗亦孝)[1,2,1)], J. H. Hamilton[1], J. O. Rasmussen[2], A. V. Ramayya[1], C. Goodin[1], A. V. Daniel[1,3,4], N. J. Stone[5,6], S. J. Zhu(朱胜江)[1,7], J. K. Hwang[1], S. H. Liu(刘少华)[1], C. J. Beyer[1], Ke Li(李 科)[1], H. L. Crowell[1], D. Almehed[8], S. Frauendorf[8,9], A. Covello[10], V. Dimitrov[11], Jing-ye Zhang(张敬业)[6], X. L. Che(车兴来)[7], Z. Jang(姜 卓)[7], D. Fong[1], A. Gelberg[12], I. Stefanescu[13], A. Gargano[10], E. F. Jones[1], P. M. Gore[1], I. Y. Lee[2], G. M. Ter－Akopian[3], Yu. Ts. Oganessian[3], M. A. Stoyer[14], R. Donangelo[15], W. C. Ma(马文超)[16], J. D. Cole[17], J. Kormicki[1], X. Q. Zhang(张学谦)[1], S. C. Wu[18], J. Gilat[2], T. N. Ginter[2,19], S. J. Asztalos[20]

(1 Physics Department, Vanderbilt University, Nashville, TN 37235, USA;
2 Lawrence Berkeley National Laboratory, Berkeley, CA 94720, USA;
3 Flerov Laboratory for Nuclear Reactions, JINR, Dubna, Russia;
4 Joint Institute for Heavy Ion Research, Oak Ridge, TN 37831, USA;
5 Department of Physics, Oxford University, Oxford OX1 3PU, United Kingdom;
6 Department of Physics and Astronomy, University of Tennessee, Knoxville, Tennessee 37996, USA;
7 Physics Department, Tsinghua University, Beijing 100084, China;
8 Department of Physics, University of Notre Dame, Notre Dame, IN 46556, USA;
9 Institut für Strahlenphysik, FZD-Rossendorf, Postfach 510119, D-01314 Dresden, Germany;
10 Dipartimento di Scienze Fisiche, Universita di Napoli Federico II, and Istituto Nazionale di Fisica Nuclear, Complesso Universitario di Monte S. Angelo, Via Cintia, 80126 Napoli, Italy;
11 Idaho Accelerator Center, Idaho State University, Pocatello, ID-83209-8263, USA;
12 Institut für Kernphysik, Universität zu Köln, 50937 Köln, Germany;
13 Department of Chemistry and Biochemistry, University of Maryland, MD 20742, USA;
14 Lawrence Livermore National Laboratory, Livermore, CA 94550, USA;
15 Instituto de Fisica, Facultad de Ingeniería, C. C. 30, 11300 Montevideo, Uruguay;
16 Mississippi State University, Drawer 5167, Mississippi State, MS 39762, USA;
17 Idaho National Laboratory, Bldg. IRCPL, MS2114, Idaho Falls, ID 83415, USA;
18 Department of Physics, National Tsing Hua University, Hsinchu, Taiwan 30013, China;
19 National Superconducting Cyclotron Laboratory, Michigan State University, East Lansing, Michigan 48824, USA;
20 Massachusetts Institute of Technology, Cambridge, Massachusetts 02139, USA)

摘 要(第一和第二部分)：使用 Gammasphere 多探测器系统对 ^{252}Cf 裂变源瞬发 γ 射线进行 γ-γ-γ 和 γ-γ(θ)符合测量，裂变丰中子原子核核结构若干前沿领域的深入研究获得了新的进展。高达 5.7×10^{11} 以上的三重和更高重符合事件的数据统计，以及更少压缩的三维数据为宽广未知丰中子核区的寻找和研究提供

* **收稿日期**：2010 - 04 - 07；**修改日期**：2010 - 05 - 03

* **基金项目**：美国能源部基金资助项目（DE-FG05-88ER40407，DE-FG02-96ER40983，DE－FG02－95ER40093)；合同资助项目(W-7405-ENG48，DE-AC03-76SF00098，DE-AC07-76ID01570)；在清华大学开展的工作为中国国家自然科学基金资助项目(10575057，10775078)；国家重点基础研究发展规划资助项目(2007CB815005)

1) E-mail：yxluo@lbl.gov

了有利的条件。在具有重要物理意义的若干丰中子核区首次建立，或显著扩展了一批包括转晕态和转晕附近能态的高自旋能级纲图。

在偶-偶丰中子核 ^{110,112}Ru 和 ^{108}Mo 中鉴别出了手征对称破缺结构。丰中子 ^{110,112}Ru 附近核的三轴形变基态具有最低的能量，在它们之中已确认了接近最大值的三轴形变。在这些 Ru 和 Mo 同位素中观察到的手征双线能带展示出手征破缺的一切特征，特别是其理想的能量简并，表明它们在迄今已报道的手征破缺结构中，具有最好的手征特性。研究了手征结构从具有 γ 软度的 ^{108}Ru 到具有大三轴形变的 ^{110,112}Ru 的过渡。斜轴推转(TAC)和随机相近似(RPA)理论计算成功地拟合了在这些偶-偶丰中子核中观察到的手征双线能带的特性，并指定其为软手征振动态。在这些偶-偶核中观察到的手征破缺不可能归纳为奇-奇核中那样的简化的几何图像。前者来自闭壳外所有中子的相互作用。

对双幻核 ^{132}Sn 附近 $N=83$ 同中素链的系统研究为这个极富吸引力的核区提供了大量新的谱学信息。$N=83$ 同中素 ^{135}Te($Z=52$)，^{136}I($Z=53$)，^{137}Xe($Z=54$)，^{138}Cs($Z=55$) 和 ^{139}Ba($Z=56$)的最新能级信息，特别是首次建立的^{138}Cs 高自旋能级纲图和壳模型理论计算表明，$Z=50$ 质子闭壳外少数 $g_{7/2}$ 价质子激发同 $N=82$ 中子闭壳外之唯一 $f_{7/2}$ 价中子的耦合对该核区能级结构具有关键作用。观察到了^{132}Sn 和^{208}Pb 附近核区谱学信息的相似性和相对应的三粒子和五粒子态。在^{135}Te 中观察到了磁转动，这是在双幻核^{132}Sn 附近观察到的首例磁转动。

关 键 词(第一和第二部分)：丰中子核；高自旋；转晕态；裂变；^{252}Cf；γ 射线三重符合；角关联；Gammasphere 多探测器系统；手征对称破缺；三轴形变；斜轴推转(TAC)计算；软手征振动；$N=83$ 同中数链；双幻核 ^{132}Sn；壳模型计算；磁转动；谱学相似性